Supplement of Geosci. Model Dev., 18, 3735–3754, 2025
https://doi.org/10.5194/gmd-18-3735-2025-supplement

Geoscientific Model Development
Open Access

Supplement of

Wastewater matters: incorporating wastewater treatment and reuse into a process-based hydrological model (CWatM v1.08)

Dor Fridman et al.

Correspondence to: Dor Fridman (fridman@iiasa.ac.at)

Model calibration

The models were calibrated separately for each calibration scenario S0, S1, and S2, allowing us to assess the contribution of the WTRM to model performance, considering both basic and advanced model setups. Improved model performance is observed across multiple metrics (KGE, NSE, and R^2) already as a result of including a simple representation of the wastewater collection and reuse (see Figure S1 and Figure S2). Further, the advanced run achieves a significant improvement, where the share of urban runoff collection into the sewers is used for calibration (Figure S3; KGE = 0.66; NSE = 0.55, R^2 = 0.58).

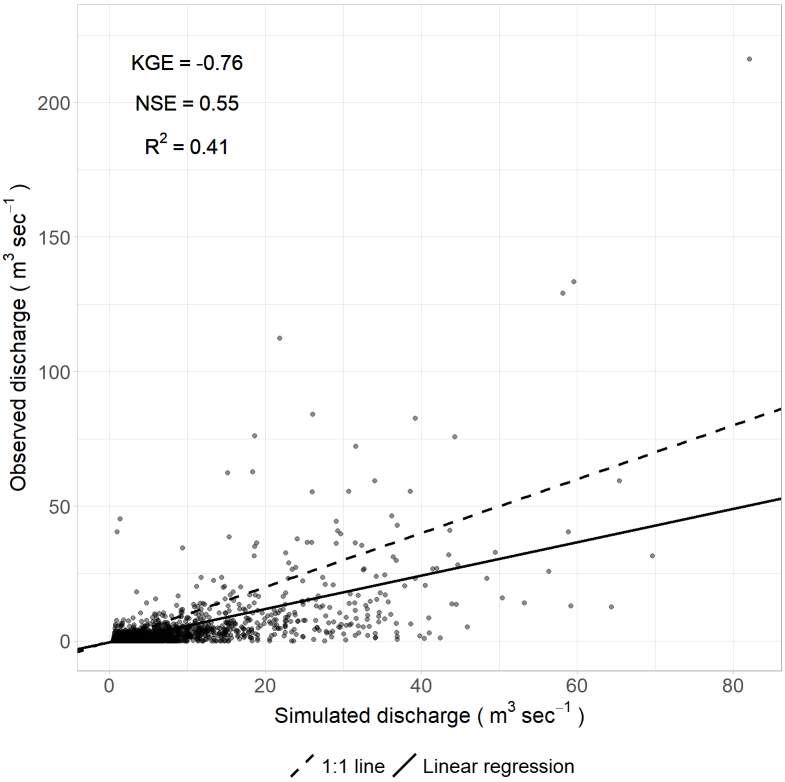

Figure S1: scatter plot of the simulated and observed discharge between 1/1/1995 – 31/12/2019 for scenario S0 (No wastewater).

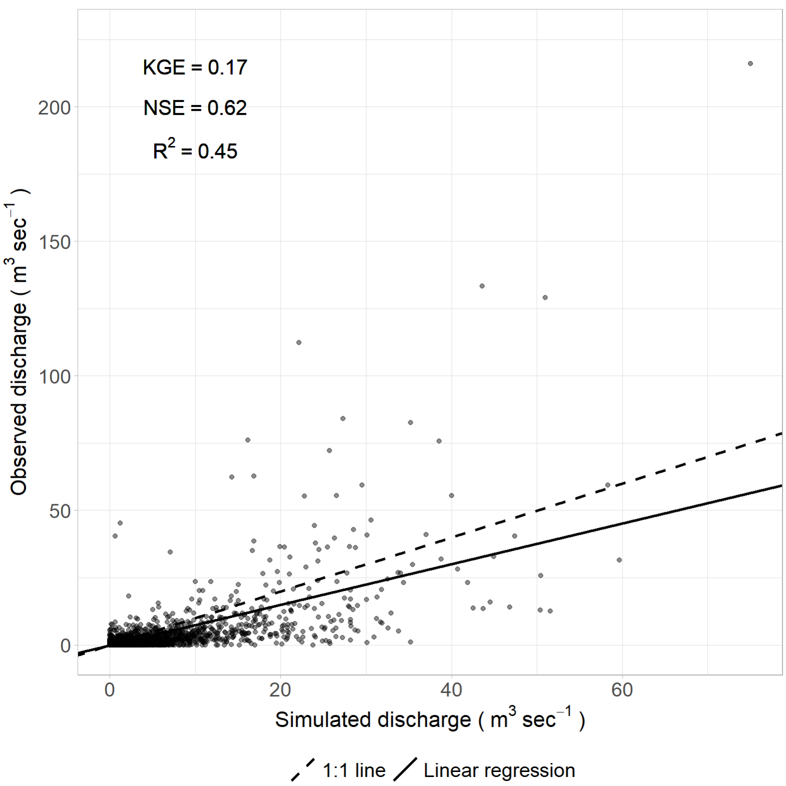

Figure S2: scatter plot of the simulated and observed discharge between 1/1/1995 – 31/12/2019 for scenario S1 (Wastewater treatment and reuse without urban runoff collection).

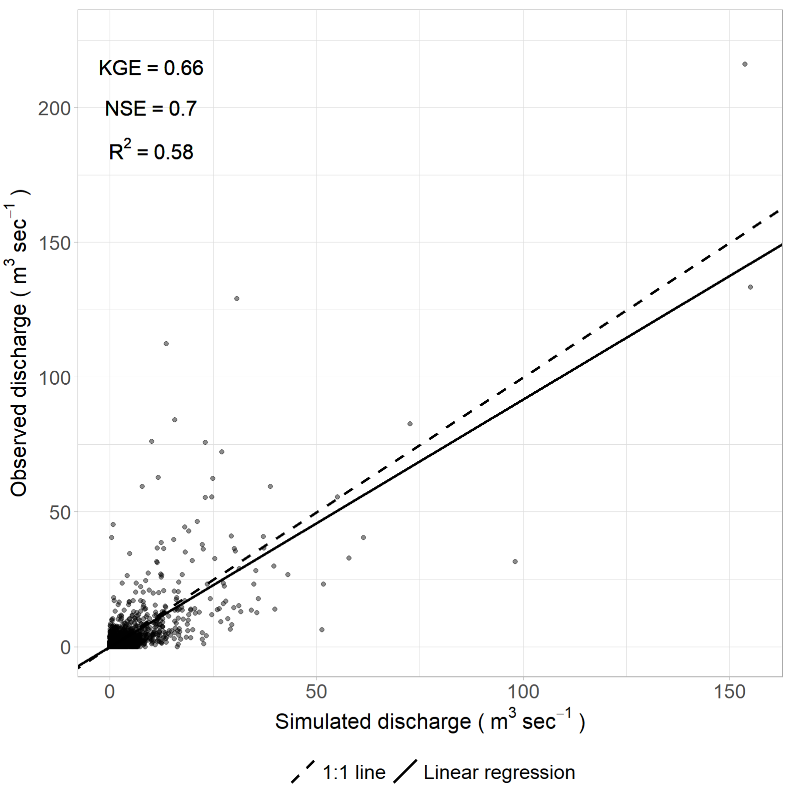

Figure S3: scatter plot of the simulated and observed discharge between 1/1/1995 – 31/12/2019 for scenario S2 (Wastewater treatment and reuse with urban runoff collection).

The models were calibrated using an evolutionary algorithm with KGE as an objective function over 24 generations. The initial pool of simulations (generation 0) consisted of 80 and 16 for each child generation. Initial median KGE values were higher, and convergence time was shorter for the scenarios incorporating the WTRM relative to the No wastewater scenario (S0; Figure S5); further, without including wastewater treatment and reuse (S0), the model performance is poor, where all simulations result in KGE smaller or equal than 0.41.

Water balance of the reservoirs in the Ayalon River Basin – based on the Water Circle concept

A water circle represents the water cycle within a specific region, component, and timeframe (Smilovic et al., 2024). Figure S4 presents the reservoir water balance in the Ayalon River basin between 2001-2006, totaling 62 $\times 10^6$ m^3 per year (Inputs + Outputs + Change in Storage). On an annual average, treated wastewater accounts for approximately 50% of the inputs (14.3 $\times 10^6$ m^3), yet reuse only accounts for 8% of the outputs (2.3 $\times 10^6$ m^3). It follows that evaporation losses (4.8 $\times 10^6$ m^3), leakage (to groundwater; 13.5 $\times 10^6$ m^3), and outflow (10.5 $\times 10^6$ m^3) account for 12 $\times 10^6$ m^3. These losses are associated with the Mesilat Zion reservoir (see reservoir number 4 in Figure 2).

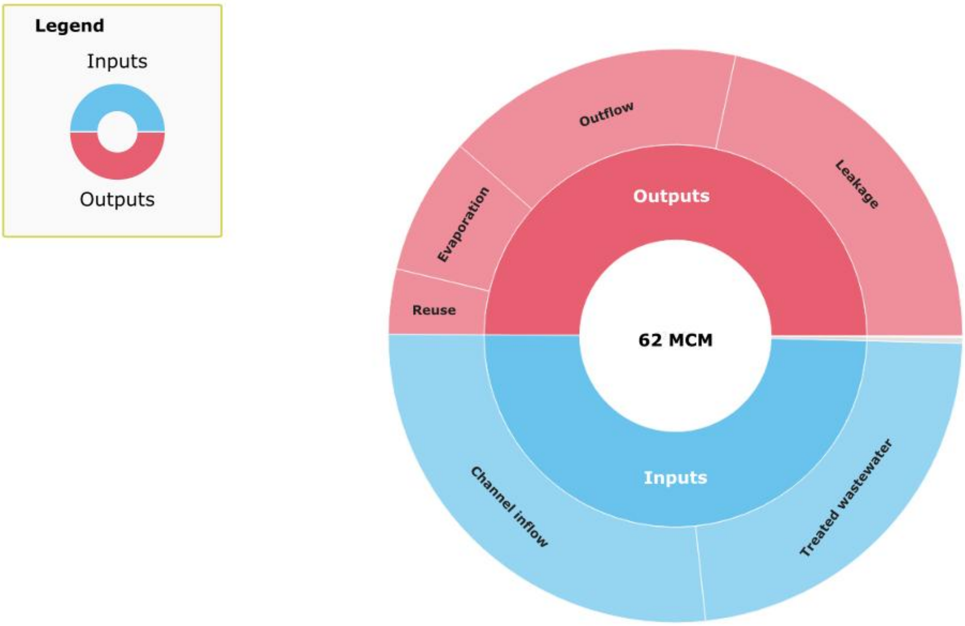

Figure S4: Average annual reservoir water balance based on a simulation for the Ayalon River Basin, Israel, from 1/1/2001 -30/07/2006, as illustrated using a water circle (Smilovic et al., 2024).

Errors associated with forcing data

The simulations presented in this manuscript were forced with meteorological data from GSWP3-W5E5 (Lange, Mengel, Treu, & Büchner, 2022). However, on some occasions, input and observed data do not align. Figure S6 shows the differences between the observed daily precipitation in the Bet Dagan meteorological station located within the Ayalon basin (X = 34.8138, Y = 32.0073) and the average daily precipitation forcing the simulation. Globally, it may be considered a good fit, yet these mismatches may result in significant errors at an arid, small catchment. One example is a rain event on 27/4/2003, shown in Figure 3, where simulated discharge ranges between 4.36 m^3 sec^{-1} (scenario S0) to 0.145 m^3 sec^{-1} (S2), while observed discharge is zero. Input data on the same date overestimates precipitation by a factor of 5.2 (see Table S1).

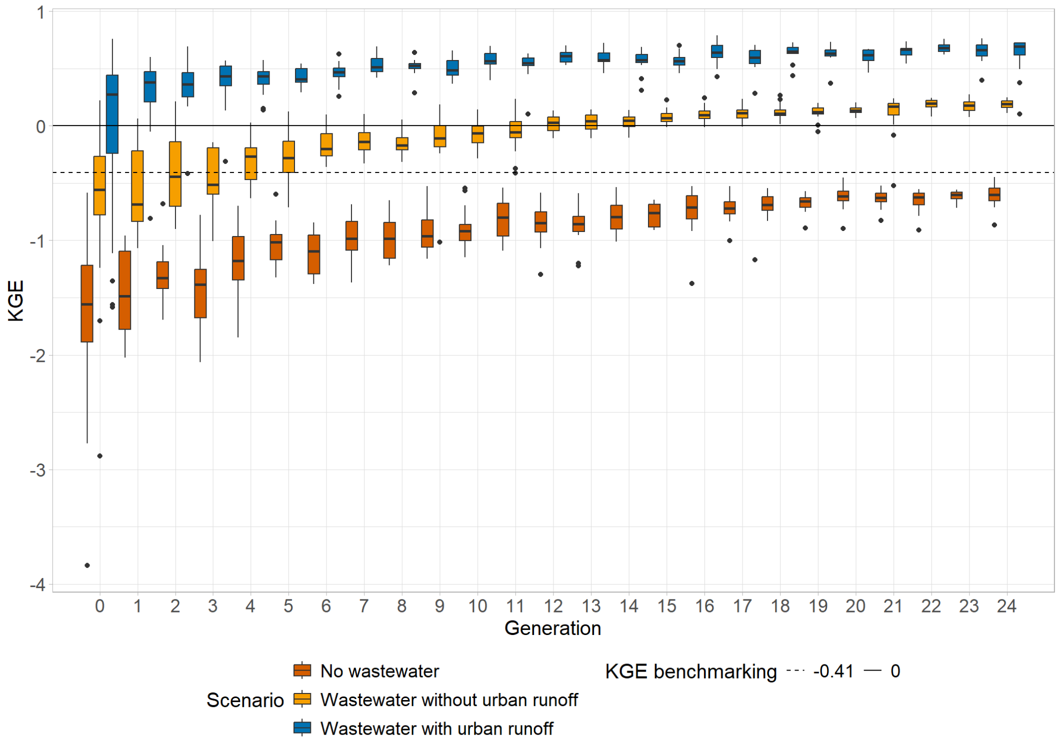

Figure S5: KGE values of simulation over generations during calibration. The boxplots show the median and interquartile range (IQR); the whiskers are estimated as a distance from the IQR, calculated as 1.6 x IQR; points stand for outliers.

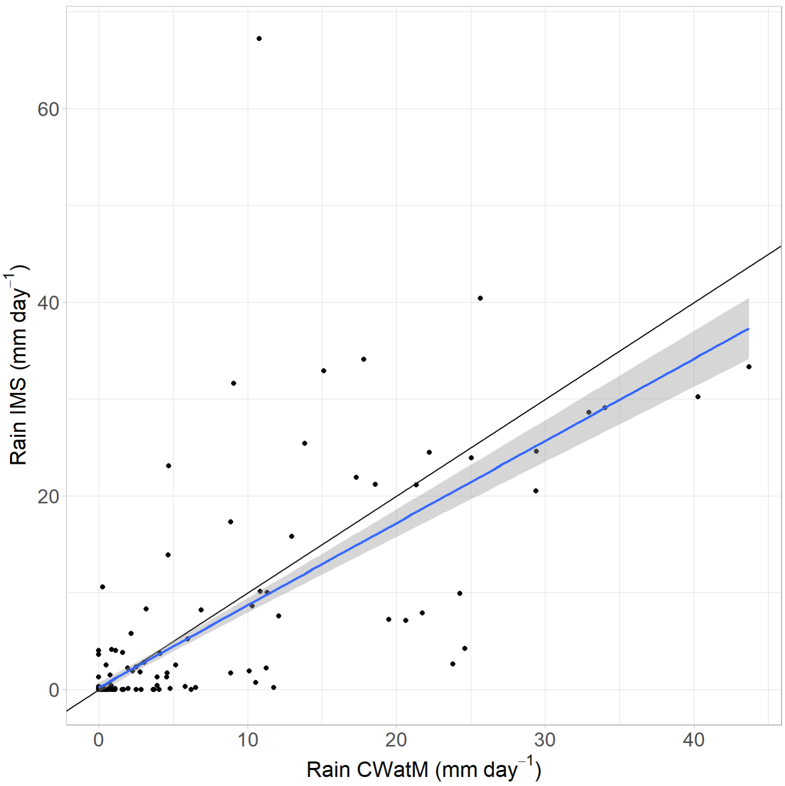

Figure S6: Comparison of forcing daily precipitation data for CWatM with observed daily precipitation data from Bet Dagan meteorological station (X = 34.8138, Y = 32.0073), representing the Ayalon basin. IMS: Israel Meteorological Service.

Dataset	**Precipitation (mm day^{-1})**
GSWP3-W5E5 (CWatM)	8.86
Observed – Bet Dagan (IMS)	1.7
Scenario	Discharge (m^3 sec^{-1})
No wastewater (S0)	4.36
Wastewater without urban runoff collection (S1)	1.64
Wastewater with urban runoff collection (S2)	0.14

Table S1: Observed and simulated precipitation and simulated discharge in the Ayalon basin on 27/4/2003. Source: Israel Meteorological Service (IMS), 2024.

<u>Validating with remote-sensing derived evapotranspiration dataset (RS-ET)</u>

As another mean of model validation, we have benchmarked the average evapotranspiration (ET) against RS-ET from various models and datasets: MOD16A2 and MOD16A2/105 (Mu et al., 2014), GLDASv2.1 (Rodell et al., 2004), and SMAP (Reichle et al., 2022). RS-ET incorporates earth observations from satellite sensors with evapotranspiration using various modeling logic, spatial and temporal scales, and diverse meteorological and remote sensing data (see Table S2). These differences often result in a range of ET estimates across time and space (Zhang et al., 2016). Elnashar et al. (2021) indicate that MOD16A2 and MOD16A2/105 are at the lower bound of ET estimates among various RS-ET, particularly in grasslands and croplands. To some extent, this can be seen also in Figure S7.

RS-ET dataset	**Remote sensing data**	**Meteorological data**	**Spatial resolution**	**Revisit time**	**Modeling logic**
SMAP	Soil moisture, leaf area index, landcover, vegetation height, soil texture, soil organic carbon	Air pressure, air temperature, precipitation, humidity, radiation, wind speed	9 km	3 hours	Land surface model
GLDAS v2.1	Soil parameters, elevation, vegetation classes	Air pressure, air temperature, precipitation, humidity, radiation, wind speed	0.25 deg (~25 km)	3 hours	Land surface model
MOD16A2, MOD16A2/105	Landcover, leaf area index, albedo, fraction of absorbed photosynthetically active radiation (FPAR)	Air pressure, air temperature, humidity, radiation, wind speed	0.5 km 1 km	8 days	Penman-Monteith, surface conductnace

Table S2: Data, resolution, and modeling logic of different RS-ET. Source: Elnashar et al. (2021), Friedl and Sulla-Menashe (2022), and Kim et al. (2023).

The simulated ET under scenarios incorporating wastewater treatment and reuse (S1 and S2) is within the range of the RS-ET from 2016 onwards (Figure S7). Comparing the simulated ET to each RS-ET across scenarios further demonstrates that incorporating the WTRM enhances performance (measured by the KGE coefficient; see Table S3).

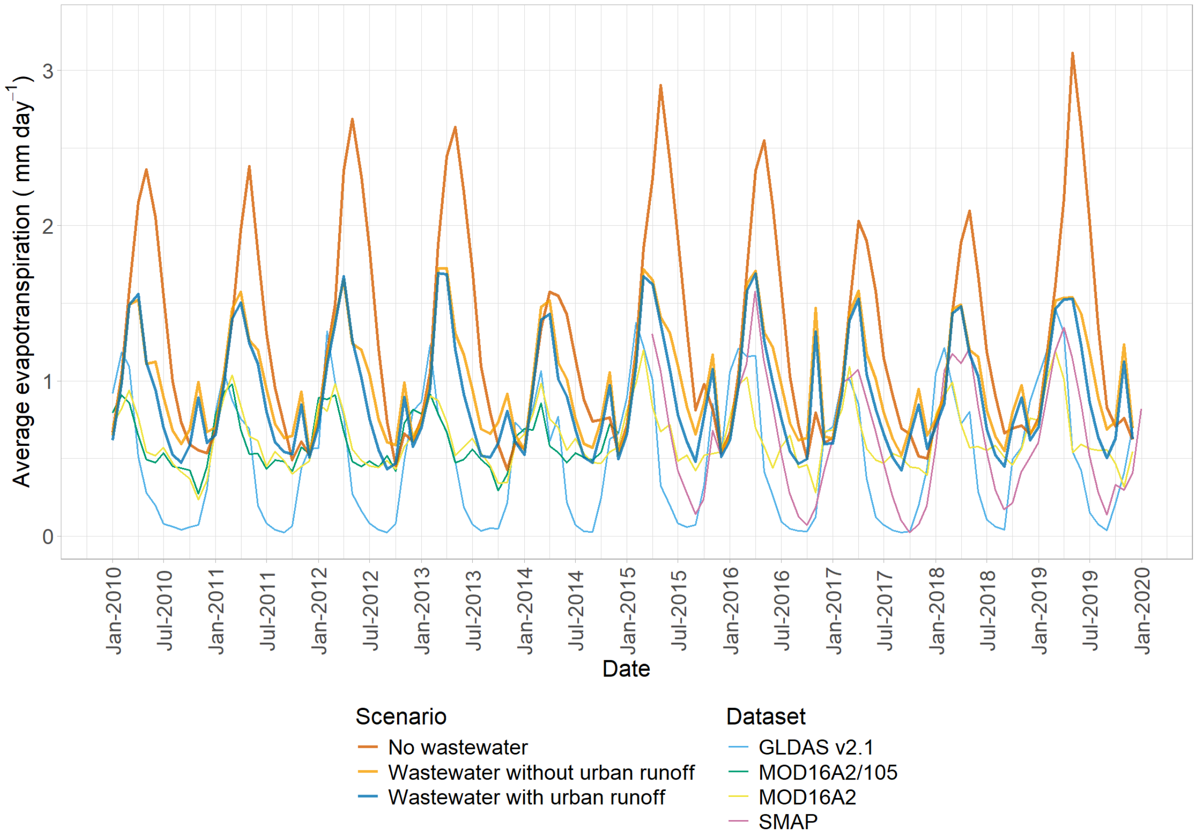

Figure S7: Comparing observed and simulated monthly terrestrial evapotranspiration (top) and seasonal gridded normalized difference for 2005. GLDAS: Global Land Data Assimilation System, SMAP: Soil Moisture Active Passive. MODIS-derived ET datasets: MOD16A2 and MOD16A2/105.

ET-RS dataset	No wastewater (S0)	Wastewater without urban runoff collection (S1)	Wastewater with urban runoff collection (S2)
GLDAS v2.1	-0.98	-0.61	-0.45
MOD16A2	-0.63	-0.15	-0.1
MOD16A2/105	-0.64	-0.2	-0.15
SMAP	-0.48	-0.1	0.01
Average ± SD	-0.68±0.18	-0.27±0.2	-0.17±0.17

Table S3: Kling-Guphta Efficiency (KGE) comparing simulated average ET to RS-ET for different scenarios and multiple RS datasets.

When comparing ET, the poor performance of the No wastewater (S0) scenario is likely associated with higher values of the 'Crop correct' and 'Reduce urban runoff' parameters. Both positively correlate with the KGE coefficients, resulting in higher simulated evapotranspiration from crops and urban areas (see Figure S8). Introducing wastewater treatment and reuse (S1) and urban runoff collection (S2) reduces discharge by diverting return flow (and urban runoff) from channels, gradually diminishing the importance of these parameters for calibration. As the correlation between the two parameters and KGE weakens under scenario S2, a clear relationship emerges between the KGE and the 'Urban leakage' parameter.

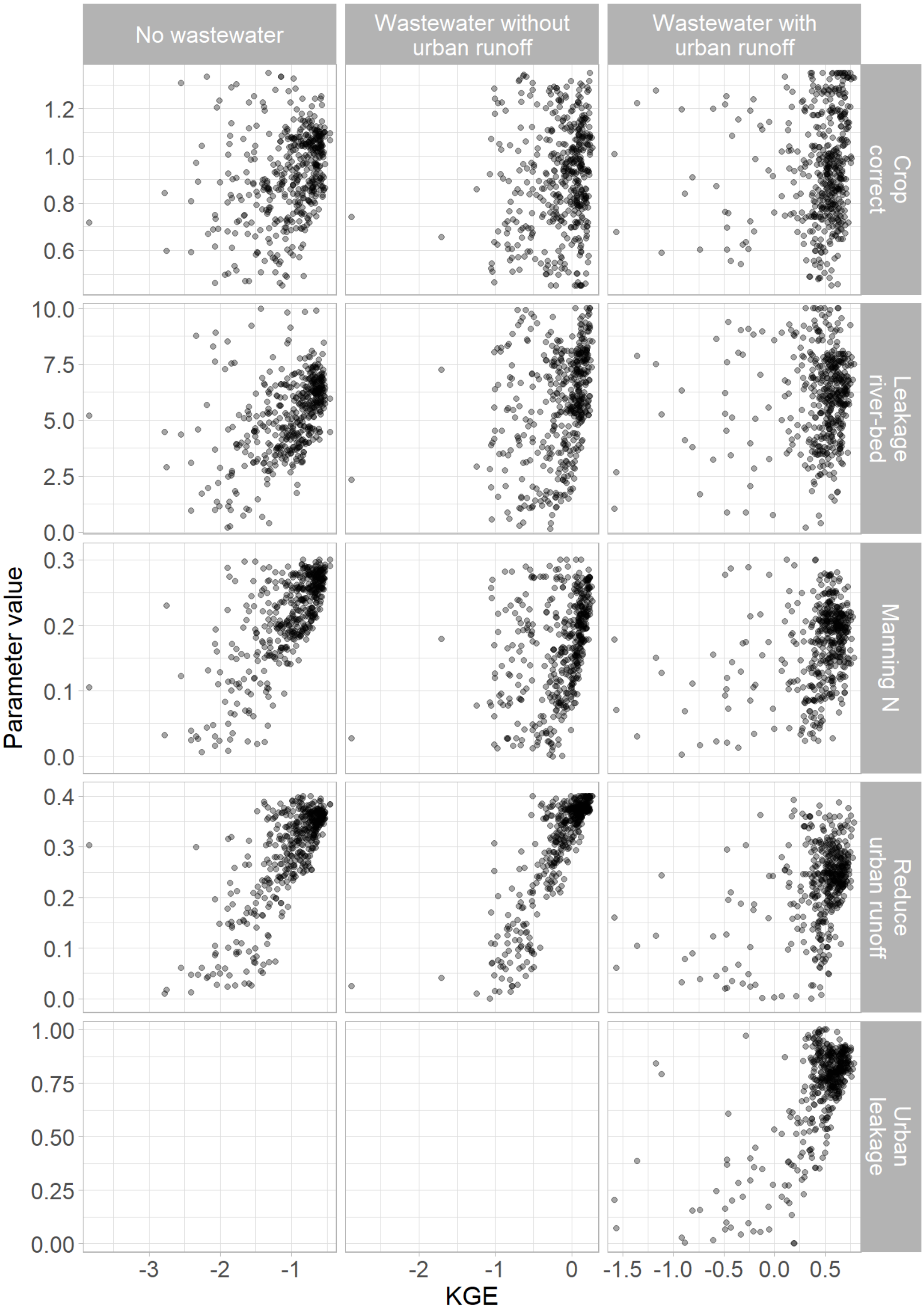

Figure S8: Scatter plots between KGE and values for selected model parameters.

Model sensitivity to the minimally allowed HRT input

The minimally allowed HRT is an optional model parameter, enabling WWTP handling of access water. Increased inflow discharge results in short residence time and may impact the removal efficiency. The relationship between hydrological retention time and inflow discharge is described using the following equation $Inflow_{max} = Volume/HRT_{min}$, where $Inflow_{max}$ is the highest acceptable inflow discharge (m^3 day^{-1}), $Volume$ is the daily treatment capacity (m^3), and HRT_{min} is the hydrological retention time (days). Information collected from annual reports of the Ayalon WWTP (Ayalon Cities Association, 2020, 2021, 2022, 2023) was used to calculate HRT_{min} using the formula above (see Table S4). To meet the changing operation conditions of the treatment plant, we replace the designed daily treatment capacity with the average daily inflow per month. Ayalon WWTP's minimal monthly HRT is 0.64±0.05 on average and at least 0.59 (January 2022). Thus, we set the minimally allowed HRT at 0.6 for scenarios S1 and S2.

Month-Year	**Average daily inflow (m^3)**	**Maximum daily inflow (m^3)**	**Minimally allowed HRT**
12-2019	60,167	97,755	0.62
2-2021	73,816	118,788	0.62
1-2022	82,964	139,726	0.59
2-2022	74,516	108,130	0.69
3-2022	73,608	120,849	0.61
11-2022	74,095	100,254	0.74
12-2022	72,789	113,211	0.64
Average	-	-	0.64±0.05

Table S4: Monthly average and peak inflows into WWTP Ayalon, calculated minimally allowed HRT during months with the highest inflows.

Simulated inflows into Ayalon WWTP are sensitive to changes in the minimally allowed HRT. The changes in the minimally allowed HRT are expressed by their inverse, indicating the maximal allowed daily inflow, which is restricted by sewage generation and collection rates. We set four different minimally allowed HRT levels as 0.001 (the lowest allowed value; multiplier equals 1000), 0.25 (multiplier is 4), 0.75 (1.33), and 1 (No access inflows are allowed; multiplier is 1). The inflows into Ayalon WWTP under each scenario are shown in Figure S9 and only occur during the wet season (October -March). We further quantify the wet season elasticity as the ratio between the relative change in inflows to the relative change in minimally allowed HRT. All sensitivity scenarios are benchmarked against the selected level of minimally allowed HRT (0.6). Except for the unlimited inflows scenario, which has very low elasticity, as it is restricted by generated and collected wastewater, the elasticity is 24%, 29%, and 33% (corresponding to the 4, 1.33, and 1 multipliers, respectively). The average elasticity is 29±4.5%, indicating that a one percent change in the minimally allowed HRT would result, on average, with a 0.29% change in the inflows. From an operative point of view, peak discharge should be restricted to prevent sludge from being washed away, making the unlimited multiplier scenario unrealistic. As such, the WTRM default minimally allowed HRT is set as one.

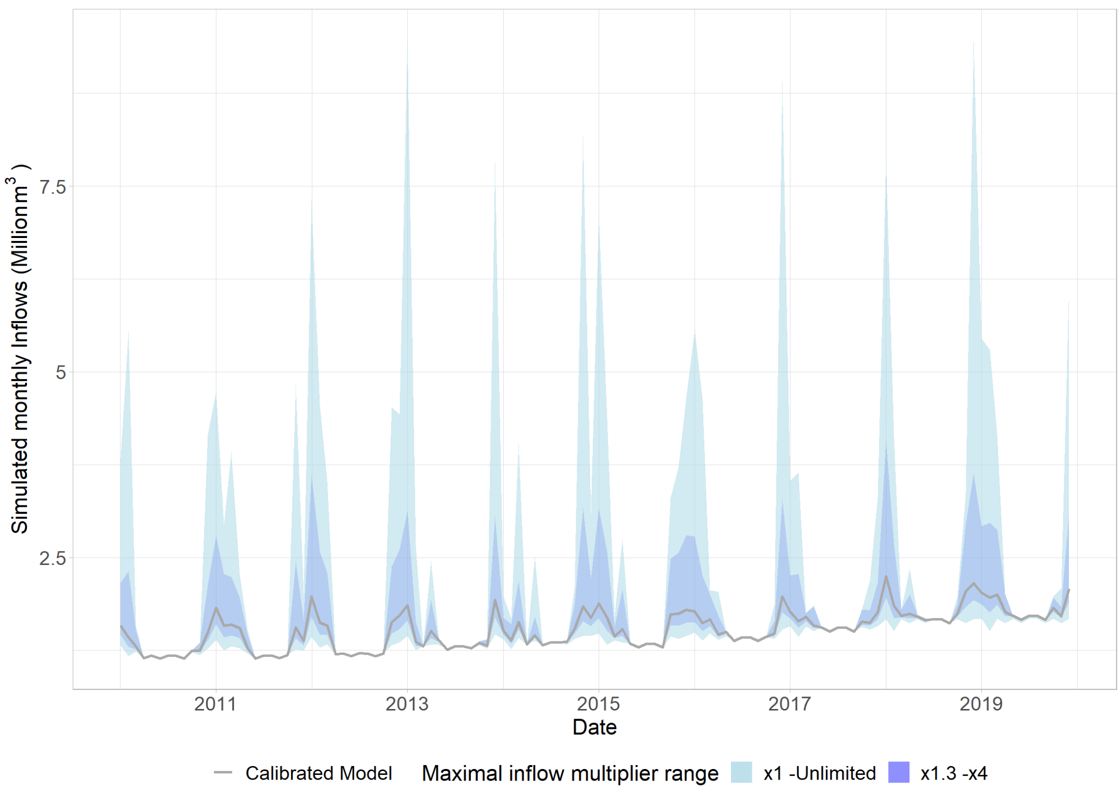

Figure S9: Sensitivity of the inflow into Ayalon WWTP to changes in the minimally allowed HRT. Maximal inflow into multiplier is expressed as the inverse to the minimally allowed HRT, indicating the maximal allowed inflow increase.

<u>Model sensitivity to the minimally allowed HRT input</u>

The model incorporating urban runoff collection (S2) better captures the inflow dynamics of wastewater into the Ayalon WWTP, yet it slightly overestimates the peak inflows (Figure 5). This improvement is supported by different metrics used for model validation, including the NSE, P-bias, and Pearson correlation (see Table S5). The average inflow of scenario S2 is also closer to the observed average inflow. According to the KGE, scenario S1 better simulates the inflow into the Ayalon WWTP, primarily due to the higher variability (coefficient of variance) of scenario S2.

Metric	**Wastewater without urban runoff collection (S1)**	**Wastewater with urban runoff collection (S2)**	**Observed**
KGE	0.18	-4.56	-
NSE	0.11	0.16	-
P-bias	-12.27	-4.56	-
Pearson correlation	0.42	0.5	-
Coefficient of variance	0.076	0.12	0.049
Average inflow (thousands m^3)	1,562	1,699	1,780

Table S5: validating the model performance regarding inflows into the Ayalon WWTP for different scenarios.

Wastewater collection areas

Figure S10 shows the wastewater collection areas (e.g., service areas) associated with the Ayalon WWTP (dotted) and the *Shafdan* WWTP (diagonal lines). This study's wastewater collection areas were derived from a national database (INRA, 2016), linking each municipality with its WWTP. The municipality borders were rasterized and assigned the identifier of each WWTP, respectively.

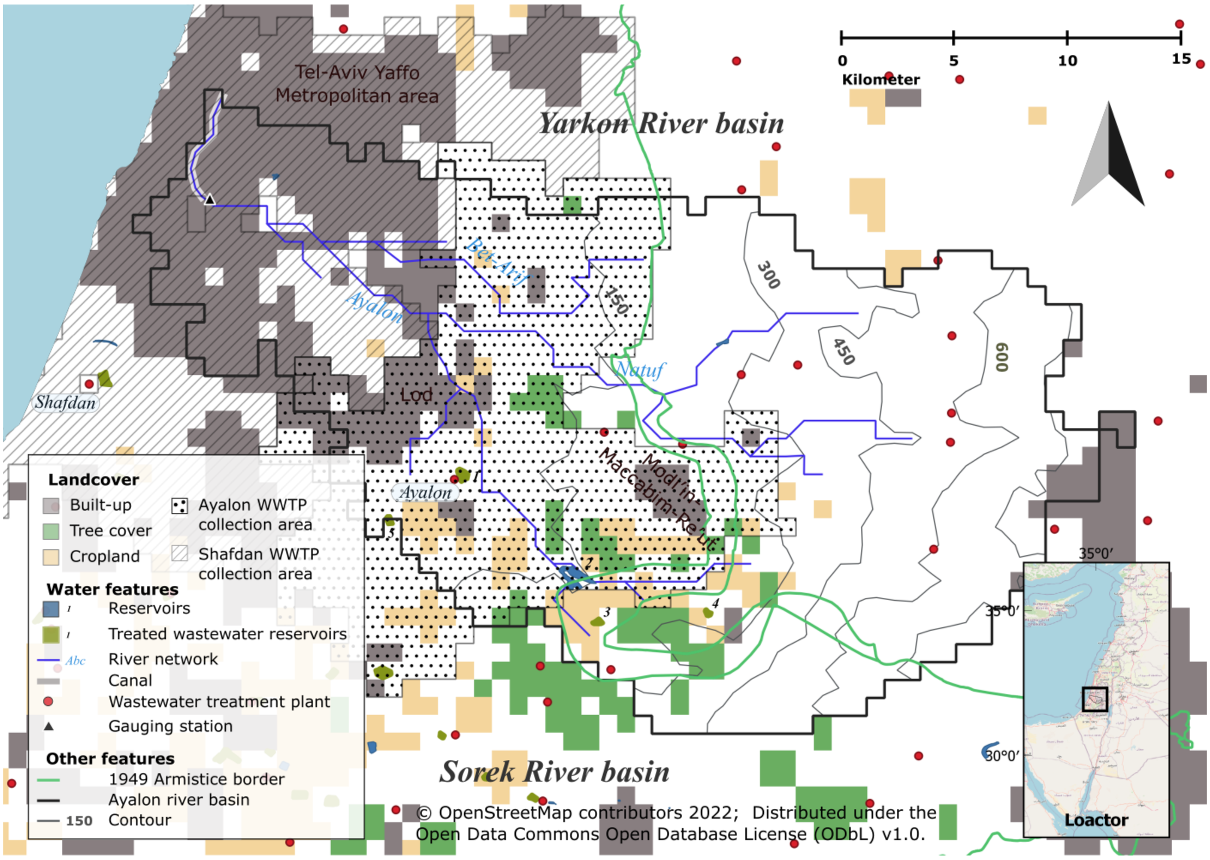

Figure S10: wastewater collection area associated with the Ayalon (dotted) and Shafdan (diagonal lines) WWTP. Partially uses data from © OpenStreetMap contributors 2022. Distributed under the Open Data Commons Open Database License (ODbL) v1.0. Marked reservoirs: (1) Ayalon; (2) Mishmar Ayalon; (3) Ta'oz; (4) Mesilat Zion; (5) Matsli'ah. Publisher's remark: please note that the above figure contains disputed territories.

Reuse scenarios – annual absolute and relative wastewater reuse

Reuse scenarios are benchmarked against the 'Wastewater and urban runoff collection' scenario (S2) between 2000-2010, comparing the share of wastewater reuse out of the total irrigation demand (see Figure S11). Wastewater reuse share of irrigation water increased significantly in 2003 due to the expansion of Ayalon WWTP's capacity from 22,000 to 54,000 m^3/day. It is also affected by climatic conditions; for example, increased precipitation during the 2006 spring resulted in lower irrigation requirements and an increased share of wastewater irrigation). Different reuse scenarios indicate quite similar irrigation shares between the two scenarios with increased storage capacity and between the other two scenarios, although slight differences are observed across years.

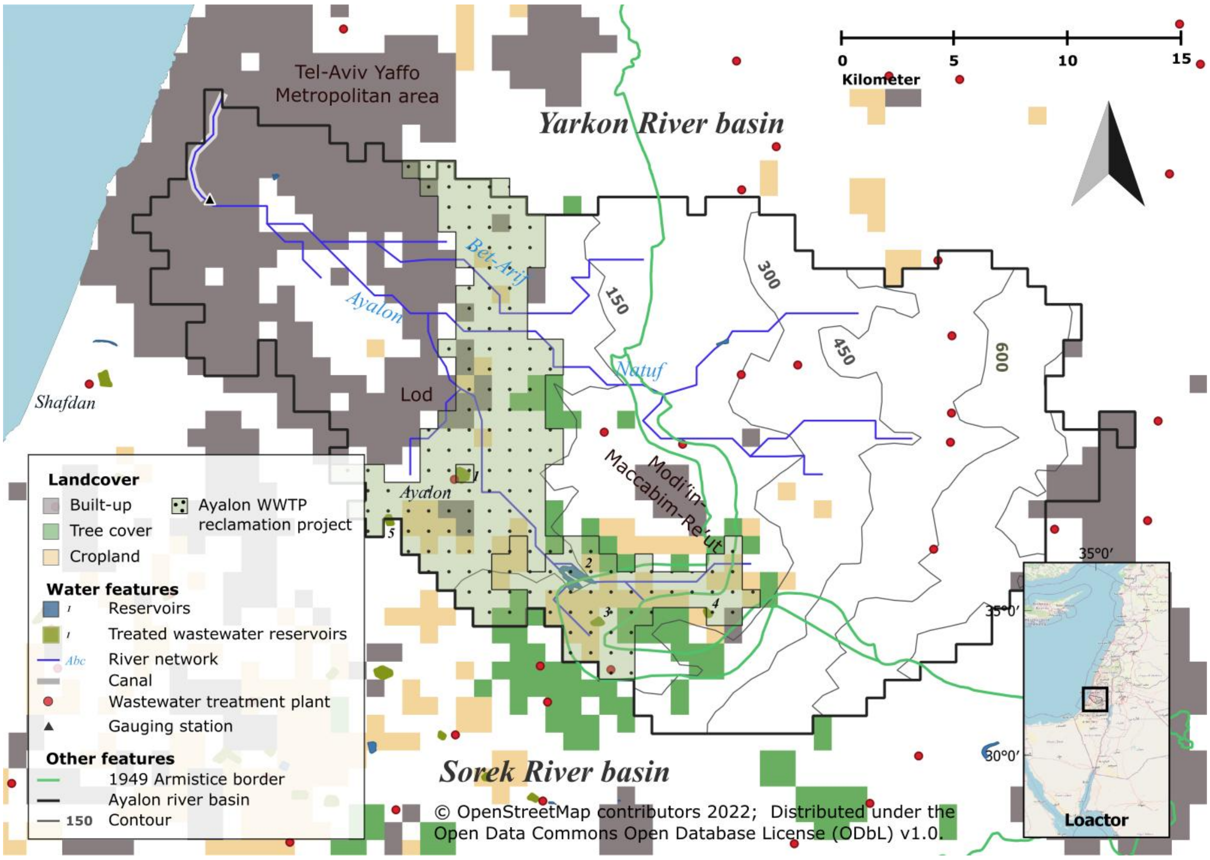

Figure S11: the Ayalon WWTP reuse project area. Partially uses data from © OpenStreetMap contributors 2022. Distributed under the Open Data Commons Open Database License (ODbL) v1.0. Marked reservoirs: (1) Ayalon; (2) Mishmar Ayalon; (3) Ta'oz; (4) Mesilat Zion; (5) Matsli'ah. Publisher's remark: please note that the above figure contains disputed territories.

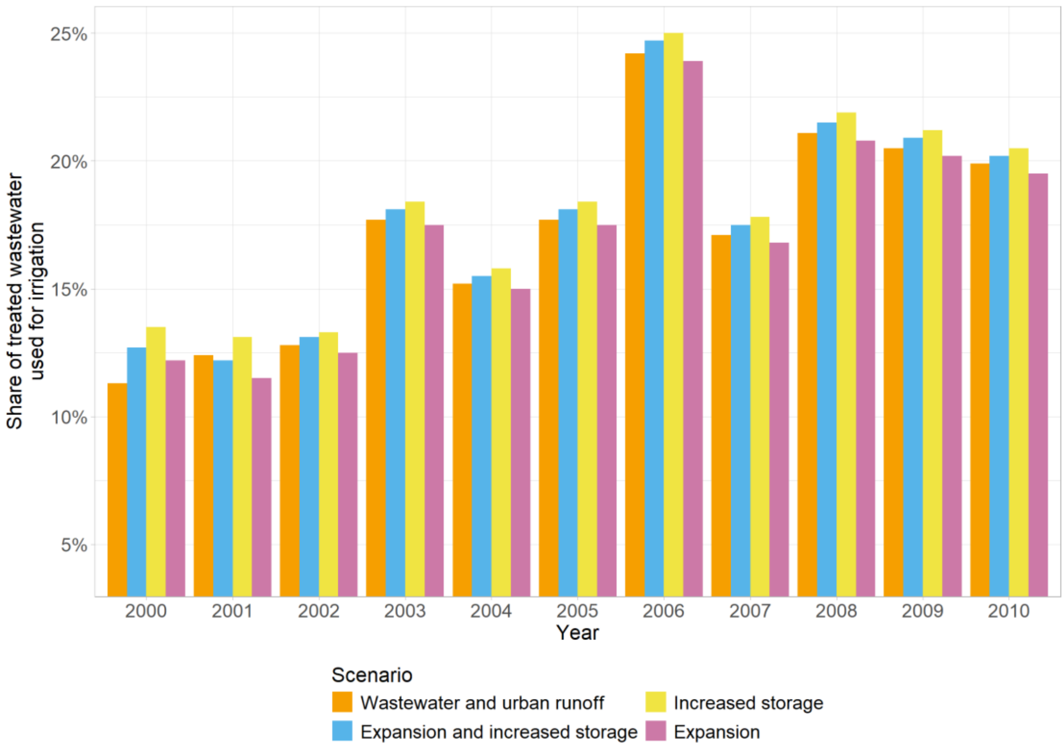

Figure S12: Percent of wastewater reuse out of irrigation demand in the Ayalon basin under different reuse scenarios between 2000 -2010.

<u>References</u>

Ayalon Cities Association.: Wastewater treatment plant Ayalon-Nesher - Annual report for 2019. https://ayalonb.co.il, last access: 3/10/2024, 2020

Ayalon Cities Association.: Wastewater treatment plant Ayalon-Nesher - Annual report for 2020. https://ayalonb.co.il, last access: 3/10/2024, 2021

Ayalon Cities Association.: Wastewater treatment plant Ayalon-Nesher - Annual report for 2021. https://ayalonb.co.il, last access: 3/10/2024, 2022

Ayalon Cities Association.: Wastewater treatment plant Ayalon-Nesher - Annual report for 2022. https://ayalonb.co.il, last access: 3/10/2024, 2023

Elnashar, A., Wang, L., Wu, B., Zhu, B., and Zeng, H.: Synthesis of global actual evapotranspiration from 1982 to 2019. *Earth Systems Science Data*, 13(2): 447-480. https://doi.org/10.5194/essd-2020-124, 2021.

Friedl, M. and Sulla-Menashe, D.: MCD12Q1 MODIS/Terra+Aqua land cover type yearly L3 Global 500m SIN Grid V006 NASA EOSDIS Land Processes DAAC [Dataset], 2019.

Israel Meteorological Service (IMS). Meteorological Databases. https://ims.gov.il/en/data_gov, last accessed: 1-10-2024, 2024.

Kim, Y., Park, H., Kimball, J. S., Colliander, A., and McCabe, M. F. Global estimates of daily evapotranspiration using SMAP surface and root-zone soil moisture. *Remote Sensing of Environment*, 289: 113803. https://doi.org/10.1016/j.rse.2023.113803, 2023.

Lange, S., Mengel, M., Treu, S., and Büchner, M.: ISIMIP3a atmospheric climate input data. ISIMIP Repository [Dataset]. https://doi.org/10.48364/ISIMIP.982724, 2022.

Mu, Q., Maosheng, Z. Running, S. W., and Numerical Terradynamic Simulation Group.: MODIS Global terrestrial evapotranspiration (ET) product MOD16A2 collection 5 [Dataset], 2014.

Reichle, R.H., De Lannoy, G., Koster, R.D., Crow, W.T., Kimball, J.S., Liu, Q., and Bechtold, M.: SMAP L4 Global 3-hourly 9 km EASE-Grid Surface and Root Zone Soil Moisture Analysis Update, Version 7. [Indicate subset used]. Boulder, Colorado, USA. NASA National Snow and Ice Data Center Distributed Active Archive Center. doi:10.5067/LWJ6TF5SZRG3, 2022.

Rodell, M., Houser, P.R., Jambor, U., Gottschalck, J., Mitchell, K., Meng, C.-J., Arsenault, K., Cosgrove, B. , Radakovich, J., Bosilovich, M., Entin, J.K., Walker, J.P., Lohmann, D., and Toll, D..: The Global Land Data Assimilation System, *Bull. Amer. Meteor. Soc.*, 85(3), 381-394. https://doi.org/10.1175/BAMS-85-3-381, 2004.

Smilovic, M., Burek, P., Fridman, D., Guillaumot, L., de Bruijn, J., Greve, P., Wada, Y., Tang, T., Kronfuss, M., and Hanus, S.: Water circles-a tool to assess and communicate the water cycle. *Environ. Res. Lett.*, 19: 021003. https://doi.org/10.1088/1748-9326/ad18de, 2024.

Zhang, K., Kimball, J. S., and Running, S. W.: A review of remote sensing based actual evapotranspiration estimation. *WIREs Water*, 3: 834-853. https://doi.org/10.1002/wat2.1168, 2016.